Atmospheric pressure continuous flow methane oxidation to methanol and acetic acid using H_2O_2 over Au-Fe catalyst

Anuradha V Jagtap[a†$], Pawan Kumar[a†$], Sharad Gupta[a], N. Abharana[b], S.N. Jha[b], D. Bhattacharyya[b], T. G. Ajithkumar[c] and C. P. Vinod[a†*]

[$] Both the authors contributed equally to this work

[a] Catalysis and Inorganic Chemistry Division, CSIR-National Chemical Laboratory, Dr. Homi Bhabha Road, Pashan, Pune- 411008, India.

[†] Academy of Scientific and Innovative Research (AcSIR), Ghaziabad, 201002, India

[b] Atomic and Molecular Physics Division, Bhabha Atomic Research Centre (BARC), Mumbai-400085, India

[c] Physical and Materials Chemistry Division and Central NMR Facility, CSIR-National Chemical Laboratory, Dr.Homi Bhabha Road, Pune- 411008, India.

* Phone No.:+91-20-2590-2086, Email: cp.vinod@ncl.res.in

KEYWORDS. Methane, methanol, acetic acid, continuous flow oxidation, Au-Fe silica catalysts, synergistic effect

ABSTRACT: An enormous value proposition exists when molecules like acetic acid and methanol are derived from natural gas. With abundant worldwide resources, methane to methanol (M2M) by partial oxidation or acetic acid through C-insertion is considered one of the catalysis's most enterprising chemical transformations. In this work, significant catalytic challenges successfully tackled are the continuous partial oxidation of methane to methanol and acetic acid at atmospheric pressure. In continuous flow and at atmospheric pressure, a modified silica-supported bimetallic (AuFeHS) catalyzed methane to methanol using H_2O_2 with an impressive yield of 224 mmol/g_{Fe+Au}. Co-feeding CO in the stream produces acetic acid, demonstrating a selectivity switch from methanol with an overall yield of 92 mmol/g_{Fe+Au}.

Methane is one of the major constituents of natural gas, and its presence in waste landfills and manure feedstocks adds to the potential list of chemicals contributing to global warming[1]. Methane has a high calorific value and can be directly used as fuel, but its storage and transportation are not practical as it needs to be compressed to 10-100 atm for commercial utility. Alternatively, CH_4 is converted into chemicals using an indirect route involving synthesis gas ($CO+H_2$) [2]. Methane is envisaged to have tremendous potential to be a raw material that can be converted into various high-value chemicals. One of the biggest obstacles in this direction is the activation of non-polar methane with a central carbon atom surrounded by four hydrogen atoms forming a regular tetrahedron, thereby requiring harsh reaction conditions[3]. A more significant challenge is the partial oxidation of methane (POM) to methanol or any other useful platform molecules, as thermodynamics suggests that an activated C-H bond is so reactive that it readily undergoes complete oxidation to CO_2. Direct conversion of methane to value-added liquid fuels and chemicals such as methanol, olefins, hydrogen, and aromatics has thus become an important research topic attracting interest from industry and academia[4,5]. Indeed, direct partial oxidation of methane to methanol is considered a holy grail problem in catalysis and is a dream reaction that still eludes the catalysis community[5–8]. In general, molecular oxygen and H_2O_2, the two green oxidants, are targeted because of their better commercialization scope, and if successful, catalytic technologies can be developed through these routes. While molecular oxygen is the ideal solution for this problem, the yields reported so far for methanol, and other oxygenates are so poor that any commercialization scope is far in sight. The new and cheaper technologies in the future for producing H_2O_2 make any catalytically oxidative pathway this molecule might offer a boon or future[9].

The development of active material for this conversion in high-pressure batch process has been explored on vari-

ous supported metal sites and metal alloys [10–14]. Wang and coworkers reported the conversion of methane over oxo dicopper anchored on carbon nitride with a methanol production of 129.7 mmol g_{Cu}^{-1} h^{-1}[10]. Hutchings and coworkers reported the production of 7.02 μmol of oxygenates in 30 min of using AuPdCu supported on titania[14]. Most of the reports suffer from low product yield and high temperature and high-pressure reaction conditions, limiting the use of the catalyst at the commercial level.

Early reports on single site catalysts for methane partial oxidation have interested researchers because the highly dispersed metal particles on various supports significantly modify their chemical and electronic properties in the materials[15–25]. Xinhe Bao and coworkers explored the various transition metal supported on graphene, confirming that the graphene-confined iron single-atom catalyst can activate the methane at room temperature and 20 bar pressure. In this report the FeN4/GN-2.7 catalyst was able to catalyze methane partial oxidation, resulting in the production of approximately 114 μmol of C1 oxygenates in 10h[18]. Song and coworkers produced synergistic catalysts with single chromium atoms supported on TiO_2 nanoparticles for direct methane oxidation to C1 oxygenated products, yielding 43.9 μmol[17]. In another report, ZSM-5-supported single Cu atoms were shown to be active and selective for methane partial oxidation with yield for C1 oxygenates of 4800 μmol·g_{cat}^{-1} within 30 min[22]. The literature suggests that most catalysts employed for methane activation suffer from low methanol selectivity, harsh reaction conditions, and material stability.

There are only limited reports for the POM to methanol in a continuous flow reactor[26–30] with most reports on using molecular oxygen as the oxidant with frugal conversion to methanol. For example, Karthik et. al. reports the production of 1.81 μmol$h^{-1}g_{cat}^{-1}$ of methanol using O_2 as an oxidant at 210 ^{o}C[26]. Hutchings and co-workers recently reported POM reaction in a high-pressure continuous process using H_2O_2 as an oxidant[27]. The yield obtained was 0.081 $mol_{Product}$ $kg_{catalyst}^{-1}$ h^{-1} at 20 bar pressure. Considering the importance of this reaction, it is highly desirable to construct a catalyst material that can activate methane at mild conditions and selectively produce desired oxygentaes. In this report, we disclose an Au-Fe catalyst supported over hydrophobic silica to partially oxidize methane to methanol using H_2O_2 (15% w/v) as an oxidant both in batch (20 bar) and continuous process (atmospheric pressure) with high selectivity. We also show that co-feeding CO with methane produces acetic acid in excellent yield. The overall conversion achieved through the atmospheric pressure continuous process in the present work is the best reported, surpassing the high-pressure batch process for methanol and acetic acid.

Results and Discussions

A modified deposition precipitation (DP) method was used to disperse atomic clusters of Fe onto hydrophobic silica (HS) support[31]. The best-performing catalyst (0.2Au0,5FeHS, further written as AuFeHS) had an optimum Fe concentration of 0.46 wt % and Au concentration of 0.23 wt %, confirmed by the Inductively Coupled Plasma-Optical Emission Spectrometry (ICP-OES). The importance of hydrophobic support in oxidation reactions involving H_2O_2 is to help peroxide close to the active sites of Au and Fe where incoming methane can react with peroxide efficiently [32–34]. Further, it is known that the active sites get blocked in the hydrophilic conditions because of the presence of moisture and it is also known that Au particle size increases in the aqueous conditions, which further lowers the activity of the catalyst[35–37]. A hydrophobic environment also facilitates easy desorption of the methanol from the surface, preventing over-oxidation.[38,39] The hydrophobicity of silica was confirmed by contact angle analysis with an observed angle of 118° (Fig. S1-2). The C-H vibration from silica confirmed the hydrophobic functionalization from HS (Fig. S3). The absence of characteristic reflections of Au and Fe from the powder XRD confirms a fine dispersion of metals over the AuFeHS catalyst (Fig. S4). This observation was expected with a low loading of the metals on the silica support. FeHS images obtained from HRTEM did not show any contrast difference characteristic of Fe particles (Fig. 1a). Atomic dispersion of Fe over the silica surface with extremely low loading could be the reason for this. However, small nanoparticles of Au (1.3- 3.0 nm) were observed in the case of AuFeHS (Fig. 1b and 1c). Such nanoparticle formation of Au is expected even at small loadings because of the higher surface energy of gold, which tends to stabilize in a larger size [40,41]. The elemental mapping further shows that the Au nanoparticles are finely dispersed over FeHS, resulting in a strongly interfaced AuFeHS catalyst (Fig. 1d, Fig. S5-7). The particle size distribution for Au on FeHS was in range of 1.4- 2.8 nm (Fig. 1e). A specific surface area of 392 m^2/g was observed for the AuFeHS catalyst using the present synthesis method (Fig. S8 and Table S1).

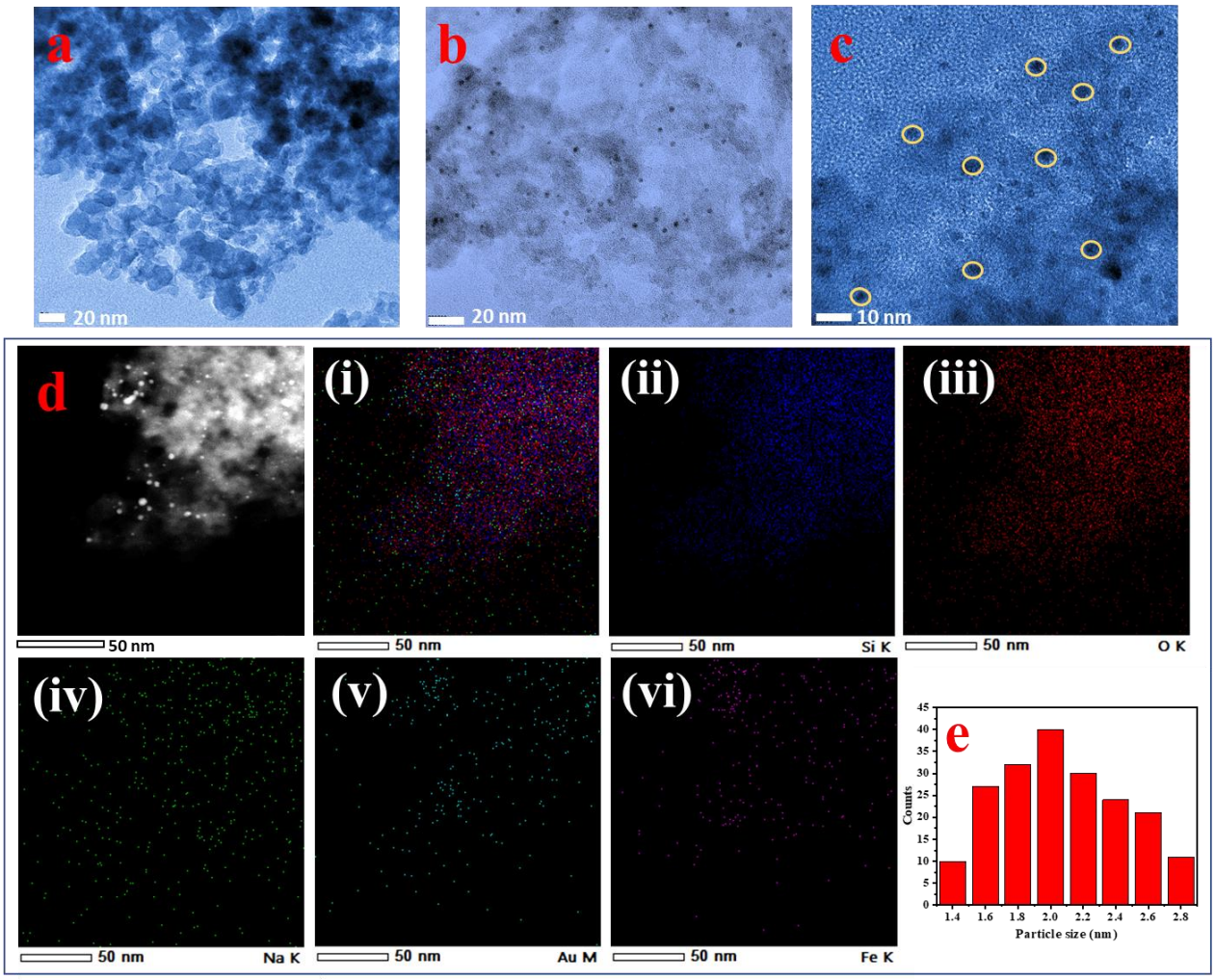

Fig. 1. a TEM images of FeHS. **b, c** AuFeHS (Scale- 20 nm and 10 nm respectively).

d Elemental mapping of AuFeHS. **e** Particle size distribution hysterogram of AuFeHS determined from TEM analysis.

X-ray photoelectron spectroscopy confirmed the oxidation state of the elements, which also gave insights into the perturbed electronic environment surrounding Fe species. C 1s spectrum recorded from both samples showed the main peak at ~285 eV corresponding to C-C and C-H fragments from the modified silica support (Fig. S9). Since the electron flood gun was used during the data acquisition, the charge correction was not required, and the BE values were reported as recorded. In Fig. 2a, Fe 2p spectra of FeHS, the presence of a peak at 710.3 eV confirms the presence of Fe^{3+} species, while the peak around 712.5 eV corresponds to FeOOH species on the catalyst surface[42]. The Fe 2p spectra of AuFeHS showed the binding energy at 710.6 eV corresponding to Fe^{3+} species (Fig. 2a)) and lower binding energy (709.5 eV) confirms the presence of low valent $Fe^{3-\delta+}$ species, which is identified as an important Fe site in methane activation [43,44]. The low valent Fe sites are also reported to be the sites for hydrogen peroxide activation by providing the OH moiety to the activated methane molecule for the formation of CH_3OH [45,46]. Over the FeHS catalyst, the low valent $Fe^{3-\delta+}$ at 709.5 eV was absent and reflected in their poor catalysis (Fig. 2a). Au 4f XPS spectra of AuFeHS (Fig. 2b) showed two peaks centered at 83.9 eV (Au 4f 7/2) and 87.6eV (Au 4f5/2) with the spin-orbit splitting difference of 3.7 eV corresponding to the binding energy of elemental gold Au0. A higher binding energy peak ~ 85 eV (4f 7/2) establishing cationic ($Au^{\delta+}$) species shows a possible charge donation and stabilization of the $Fe^{3-\delta+}$ species. Based on relative peak areas, their respective atomic percentages were estimated as 85% for Au^0, and 15 % for $Au^{\delta+}$, peaks. No considerable change was observed in the case of the Au (fresh and spent) catalyst. The cationic Au species was absent in the case of the AuHS catalyst (Fig. S10). Apart from Au and Fe, Na was also present in the catalyst and the details given in the later discussion.

Fig. 2c shows the normalized XANES spectra measured at Fe K-edge along with Fe standards. No Fe-Fe interaction was observed in the samples, revealing the single atomic nature of Fe species in the catalysts. The Fe absorption edge of the FeHS sample coincides with that of the Fe_2O_3 standard, manifesting Fe is present in the +3 oxidation state in the sample, while the low valent species of iron was observed in the AuFeHS catalyst. For the AuFeHS sample, by linear combination fitting (LCF), we could see that it has a 72% contribution of Fe_3O_4 and 28% FeO (Fig.

S11) and (Fig. S12) shows the full EXAFS (vs.) spectra of Au-Fe catalyst samples for Fe edge and Au edge respectively. Fig. S13 shows the normalized XANES spectra measured at Au L_3-edge and that of Au foil. The Au absorption edge of most samples coincides with that of Au foil, showing that Au is in an elemental state in all the samples. However, AuFeHS have an L_3 edge slightly higher than the Au metal edge possible due to some charge transfer, which is also evident as Au in cationic form as inferred from XPS. From the radial distribution functions of all samples at Fe K-edge, as shown in (Fig. 2d), the first peak appears at ~1.5Å, which is at an appreciably lower value compared to that of Fe foil. This shows that Fe is not in the elemental Fe state in the sample, as also demonstrated by XANES data discussed above (also shown in Fig. 2c). The peak at ~1.5Å corresponds to two neighbouring O shells with C.N. of 3 at 1.94 Å and 2.11Å. The best fit$\chi(R)$ versus R plots (fitting range R = 0-4 Å) of all the samples are shown in Fig. 2d, and the best-fit values are shown in Table S2.

The radial distribution functions or$\chi(R)$ versus R plots of all the samples at Au L_3-edge are shown in Fig. S14. Contrary to the Fe edge data, here the first major peak lies above 2Å and close to that of Au foil data showing that the nearest neighbor of Au in these samples are Au itself and all samples are mostly in elemental form. However, the 1st peak of AuFeHS is marginally shifted to lower R and may be due to some charge transfer, as explained by XANES and XPS.

The presence of isolated metal atoms on the surface is probed through *in-situ* IR spectroscopy (Fig. S15) [47,48]. The support shows no or little interaction with the CO molecules. The CO adsorption on Au metal atoms shows different signals for various oxidation states. There were two detectable signals in the case of Au and Fe-loaded silica near 2105, and 2175 cm^{-1}. The signal centered at 2105 cm^{-1} is assigned to terminally adsorbed Au^0-CO, whereas the signal at 2175 cm^{-1} is assigned to $Au^{\delta+}$-CO[49,50].

Catalytic activity and selectivity of Au-Fe catalysts for methane oxidation

The initial screening of all the catalysts for the partial oxidation of methane (POM) was carried out in a batch reactor at 10 bar methane pressure. The catalytic activity of hydrophobic silica (HS), monometallic Fe-HS, Au-HS, and bimetallic Au- Fe hydrophobic silica-supported catalysts was investigated. According to the previous reports, the Fe loading of less than 1 wt % is found to be optimum for efficient methane activation, so we fixed the amount of Fe as 0.5 wt % in the catalyst and varied the Au loading[51,52]. The screening of bimetallic metal loadings was carried out and the optimum was found to be 0.5 wt % Fe and 0.2 % of Au

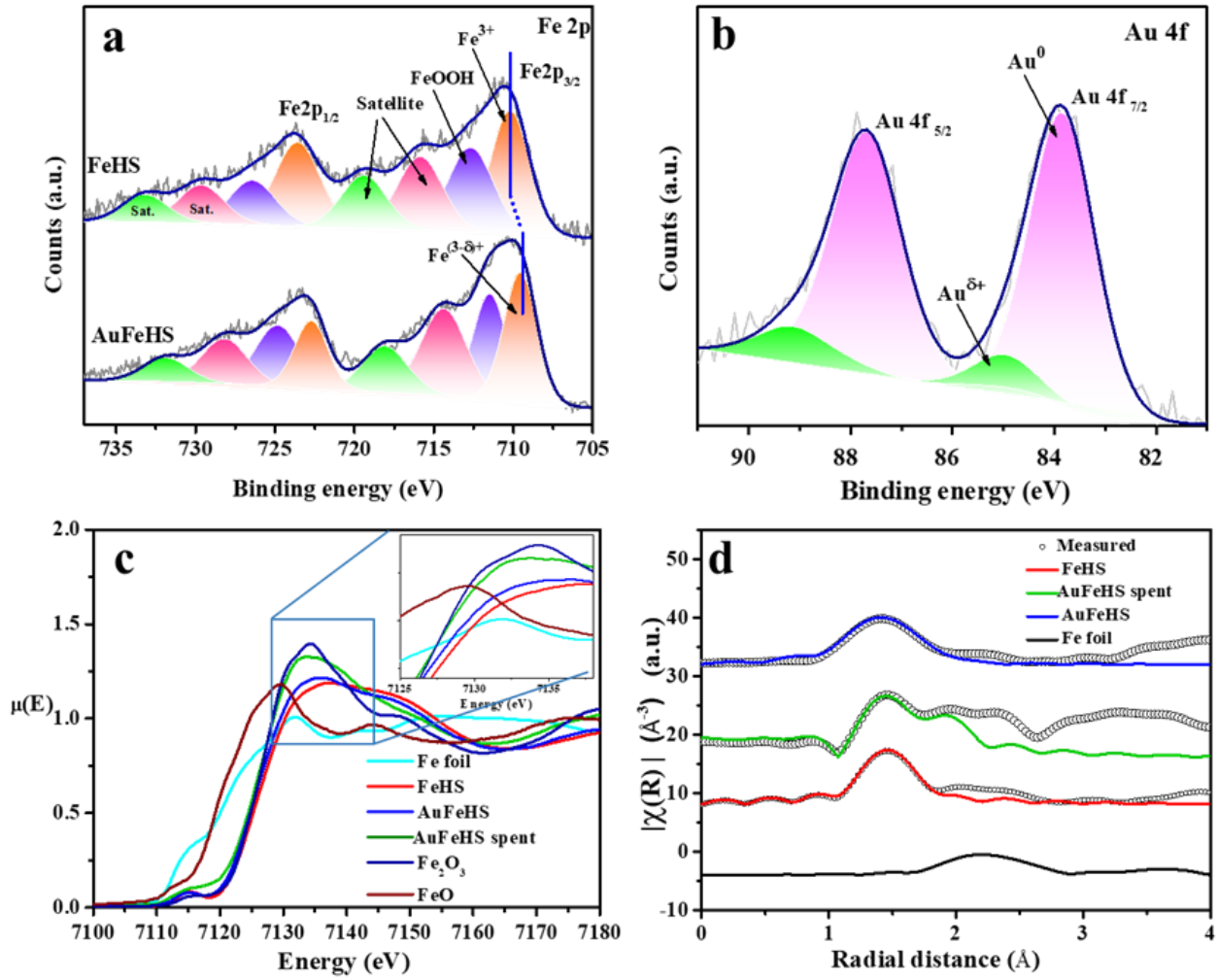

Fig. 2. Characterization of various catalysts: a and b XPS spectrum of Fe 2p and Au 4f of AuFeHS, respectively. c Normalized XANES spectra at Fe K-edge of various catalysts. d Experimental χ(R) vs. Rdata of Au-Fe catalyst measured at Fe K-edge along with best fit theoretical plots (Open circles: experimental data, solid line: theoretical best fit)

(Table S3). No product was detected for the reaction over the support (HS) (Fig. S16). The Fe-HS catalyst gave 285 mmol/g_{Fe} with a methanol selectivity of 82% from the catalyst. Under a similar reaction condition, Au-Fe HS catalyst gave a remarkable yield reaching 1666 mmol/g_{Fe+Au} with a selectivity of 95%, one of the highest selectivity reported yet[10,45]. Oxo di copper anchored on carbon nitride catalyst produced methyl oxygenates (129.7 mmol g_{Cu}^{-1} h^{-1}) at 70°C with a selectivity of 4% for methanol[10]. The other component of the catalyst, AuHS was also tested, and the yield was only 47.6 mmol/g_{Au} of methanol, showing the synergistic effects. CO_2 was observed as a side product with a selectivity of around 5%, showing 100 % selectivity for the liquid oxygenate. Optimized conditions for the efficient methanol formation were 60°C temperature and 10 bar pressure of methane (Fig. 3a and 3b). The role of the hydrophobic support can be differentiated through the activity comparison of the supports as Au and Fe supported on SBA-15 gave only 111 mmol/g_{Fe+Au} methanol under optimized conditions (Fig. 3c) (detailed comparison in Table S4). A comparison of the catalytic activity data from the Au-Fe catalyst with the best reports in the literature shows the impressive performance of this catalyst. The better yields than the presented data are from Au-Pd colloidal particles [6] and on $Cu_2@C_3N_4$ [9] supported catalysts but suffer from poor (initial) selectivity and high-pressure conditions than that reported in this work (Table S6). The control experiments done (Table S4, entries 1,2 and 3) showed that no product was detected without methane flow, oxidant and catalyst.

Stephanolpolous and co-workers showed an elegant pathway for producing acetic acid during the partial oxidation of methane by introducing CO as a co-reactant [25]. Zhong and co-workers recently reported the production of 3323 μmol/g_{cat} of total oxygenate products, with 60% acetic acid selectivity, using the CO in reactant feed [4].

Taking a cue from these reports, we carried out the methane partial oxidation in the presence of CO, and the results are shown in Fig. 3d. As intuited, there was a selectivity switch and acetic acid was formed as the main product with a yield of 3403 μmol/g_{cat} within 1h of the reaction at 50 °C in the batch process with a total gas pressure of 20 bar (15 bar CH_4:5 bar CO). Methanol was observed as the only other liquid oxygenate product formed with a yield of 166 μmol/g_{cat}. An increment in the gaseous products (CO_2) was observed with an increase in the reaction time and temperature (Fig. 3d). In the case of the AuFeHS catalyst, the CO_2 selectivity was 10 % when CO was added to the feed (Fig. 3d) at 50 °C, while 5-6 % when methane was only in the reactant feed under standardized conditions (Fig. 3b). Gas chromatography (GC) and NMR confirmed product formation, and the yield was quantified by GC using standard calibrations. A representative NMR spectrum from the reaction mixture is attached in supplementary Information (Fig. S17), where the peaks corresponding to

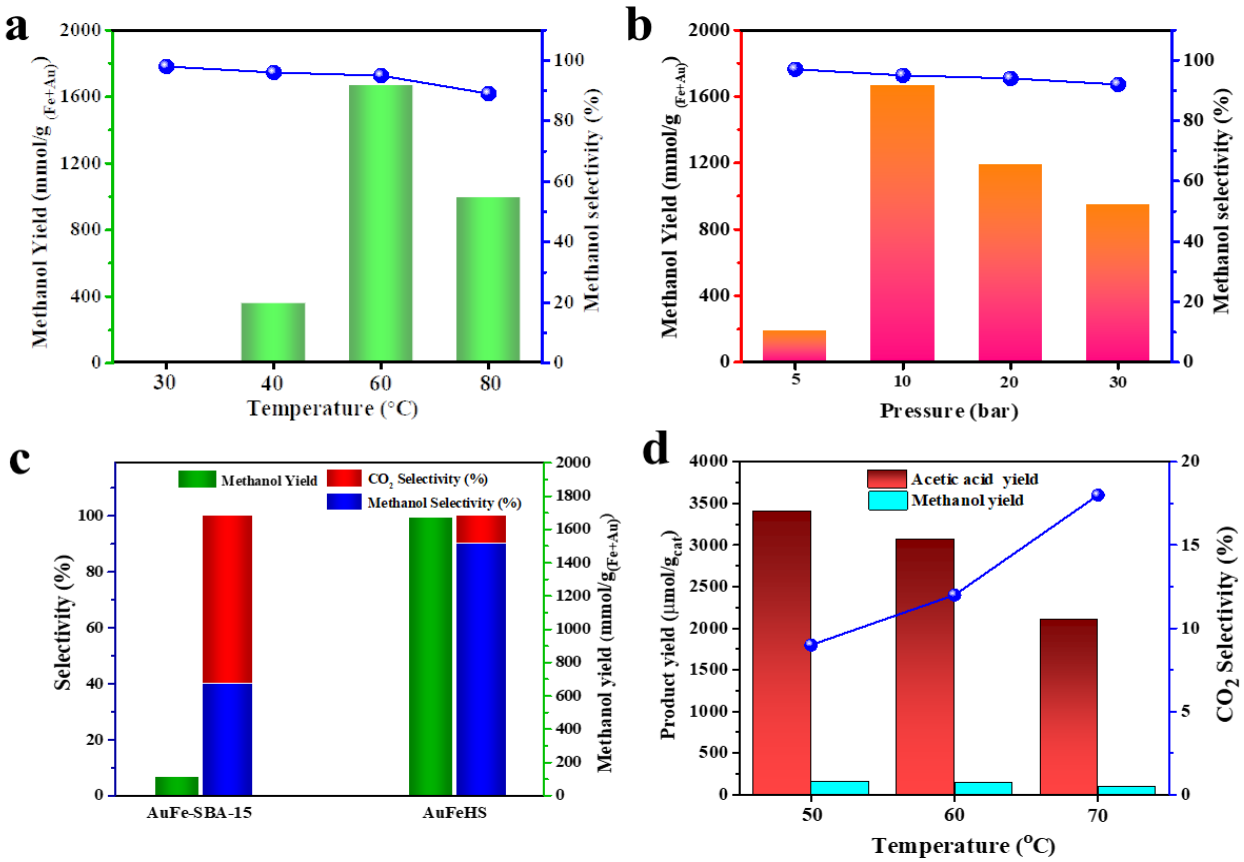

Fig. 3. Catalytic activity analysis in the batch process: **a** Catalytic activity of AuFeHS at various temperatures: Reaction conditions 25 mg catalyst, 30 min, 10 bar methane, 0.5 mL H_2O_2 (30% w/v), 20 mL H_2O, 30-80°C. **b** Catalytic activity of AuFeHS at various pressure: Reaction conditions 25 mg catalyst, 30 min, 60°C, 0.5 mL H_2O_2 (30% w/v), 20 mL H_2O, methane 5-30 bar. **c** Catalytic activity of various catalysts: Reaction conditions 25 mg catalyst, 30 min, 10 bar methane, 0.5 mL H_2O_2 (30% w/v), 20 mL H_2O, 60°C. **d** Catalytic activity of AuFeHS at various temperatures: Reaction conditions 50 mg catalyst, 1 h, 15 bar methane, 5 bar CO, 0.05 mL H_2O_2 (30% w/v), 20 mL H_2O, 50-70°C.

CH_3OH (δ= 3.3), dissolved CH_4 (δ= 0.15), and acetic acid (δ= 2.0) were observed in the NMR.

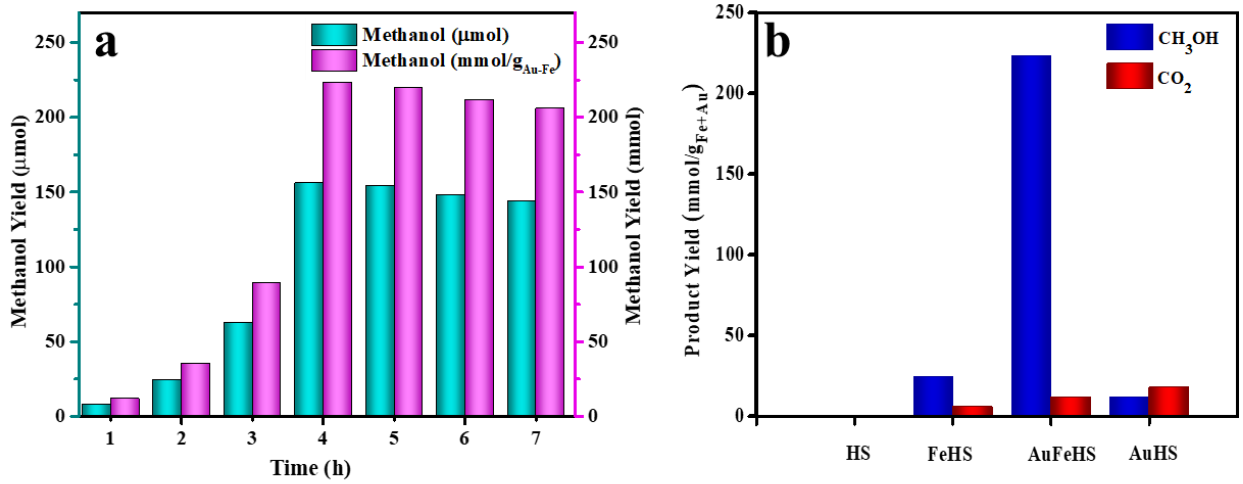

Fig. 4. Catalytic activity of various catalysts. **a** Catalytic activity of AuFeHS in continuous flow reactor upto 7h: Reaction conditions 100 mg catalyst, 80°C, 2 mL/h H_2O_2 (15% w/v) flow, methane flow 20 mL/min. **b** Catalytic activity of various catalysts in continuous flow reactor: Reaction conditions 100 mg catalyst, 80°C, 2 mL/h H_2O_2 (15% w/v) flow, methane flow 20 mL/min, 4h

Following the batch process, where excellent yield and selectivity was demonstrated for methanol and acetic during the partial oxidation of methane, we extended the POM reaction in a continuous reactor. The scheme showing the partial oxidation reaction carried out in a fixed-bed reactor in a continuous flow process at atmospheric pressure, is shown Scheme 1. The continuous flow process at atmospheric pressure for up to 7 h showed steady methanol production (Fig. 4a). The product yield reached a maximum at 4 h (157 μmol) under the optimized conditions. In the case of HS catalyst, no product was observed, while methanol was observed as the main product when metal was deposited over HS. FeHS catalyst produced 24.2 mmol/g_{Fe} of methanol while an outstanding product yield of 224 mmol/g_{Fe+Au} was reported in the case of AuFeHS. For AuHS catalyst, 12 mmol/g_{Au} was the productivity within 4 h of the reaction (Fig. 4b). The remarkable methanol yield of 422 μmol$h^{-1}g_{cat}^{-1}$ or 0.42 $mol_{methanol}$ $kg_{catalyst}^{-1}$ h^{-1} (for 4h) from the AuFeHS catalyst is better than the reported value of 1.81 μmol$h^{-1}g_{cat}^{-1}$ of methanol using O_2 as an oxidant at 210 °C[26] and 0.081 $mol_{Product}$ $kg_{catalyst}^{-1}$ h^{-1} under 20 bar pressure using H_2O_2 as an oxidant[27]. It is also exemplary because of benign conditions (atmospheric pressure) used to carry out the POM to methanol. The introduction of CO to the reactant feed results in acetic acid formation as the main product, with methanol and CO_2 as side products. 648 μmol/g_{cat} of acetic acid formed within 4 h of the reaction (Table S5, entry 2). The temperature optimization confirms that 80°C is the best condition for the effective conversion of methane at atmospheric pressure (Table S5).

The background reaction from organic groups from the catalyst, which impart hydrophobicity for the catalyst, was ruled out by carrying out the isotope (CD_4) labelling experiments on the AuFeHS catalyst. The peak at 3.3 ppm showed multiplet in ^1H NMR spectra, confirming that the methyl group in the alcohol originated from CD_4 rather than any other ligands from the support (Fig. S18). The ^2H and ^{13}C NMR spectra further confirmed the presence of labelled methanol (Fig. S19). Using nitrogen gas as feed instead of methane resulted in no products supporting the above experiment (Table S5, Entry 3). Finally, a comparison with the recent literature values for the partial oxidation of methane to methanol using H_2O_2 as an oxidant is given (Table S6). Clearly, the AuFeHS catalyst catalyzed partial oxidation of methane to methanol or acetic acid with exception yields at previously thought unfavourable conditions.

Scheme 1. Schematic illustration of catalytic reac-

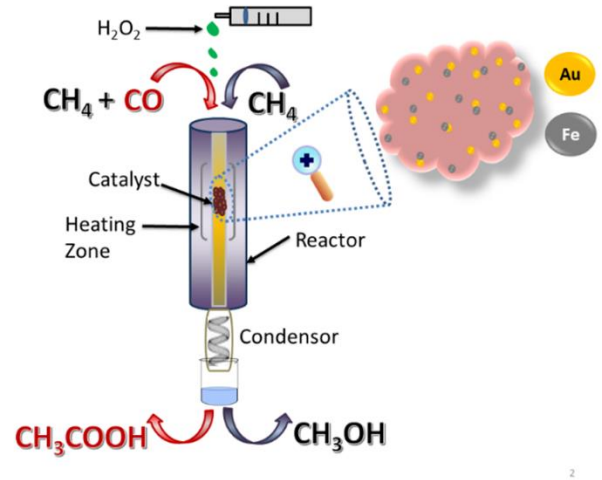

The unprecedented activity of the AuFeHS catalyst for the highly selective partial oxidation of methane to methanol and acetic acid under benign conditions could be largely understood based on the synergy between the Fe and Au, which are individually known to catalyze this reaction with H_2O_2 at high-pressure conditions. The synergistic

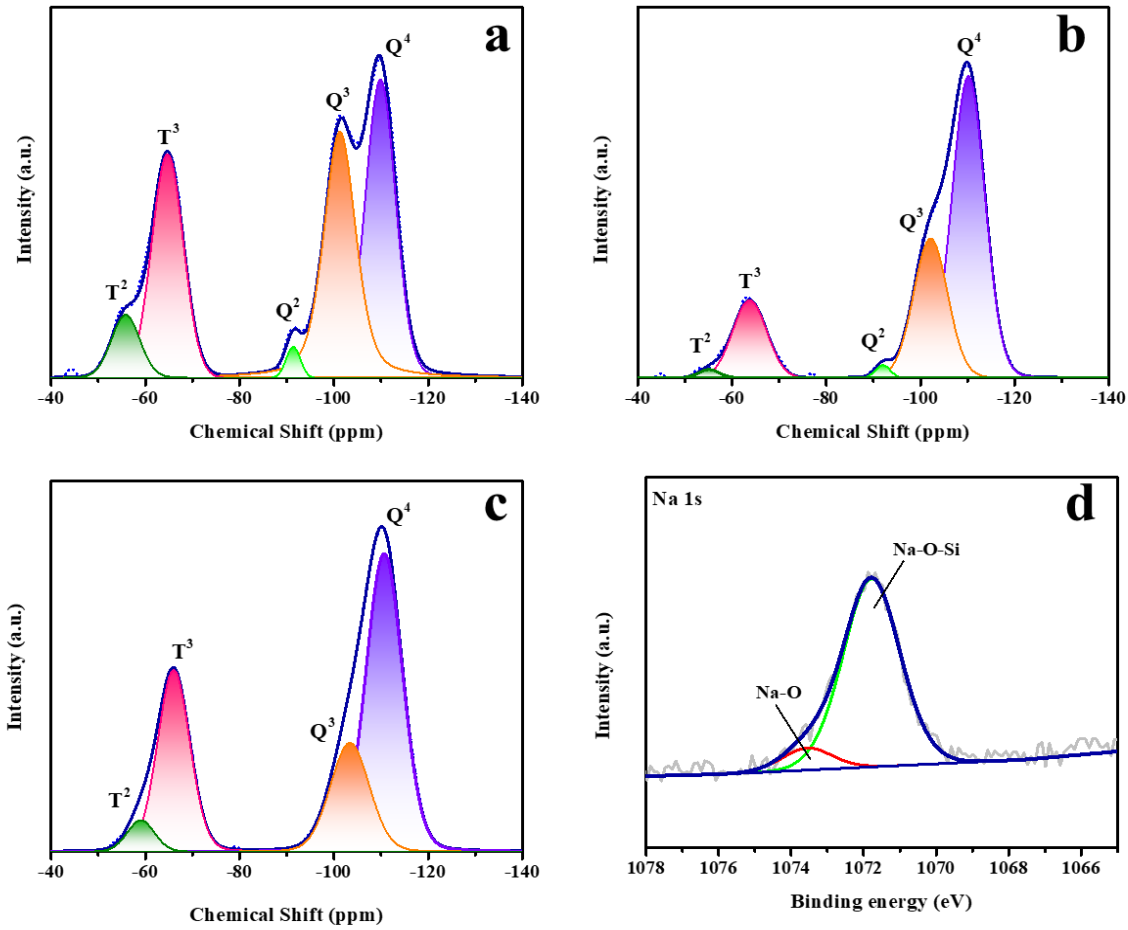

Fig. 5. Characterizations of various catalysts. **a** ^{29}Si MAS NMR spectrum of HS. **b** ^{29}Si MAS NMR spectrum of FeHS. **c** ^{29}Si MAS NMR spectrum of AuFeHS. **d** Na 1s XPS spectrum of AuFeHS.

effects between Au and Fe is also evident in the case of SBA-15 as the production of methanol (0.78 mmol/g_{cat}) was observed in the case of AuFe deposited over SBA-15 using the same synthesis method (Table S4, entry 9). Fe-SBA-15 and Au- SBA-15 was able to produce only 0.30 mmol/g_{cat} and 0.15 mmol/g_{cat} of methanol, respectively (Table S4, entry 7 & 8). Thus, the hydrophobicity of the silica and the synergistic effect are key for enhanced activity for POM reaction. One of the challenges in designing low-pressure, low-temperature methane activation catalysts is stabilizing active species, which are easily poisoned by reacting oxidants like O_2, H_2O_2, or H_2O[53]. In our case, the low valent $Fe^{\delta+}$, which can simultaneously activate both CH_4 and H_2O_2, is generated and stabilized by Au. The intimate interaction between the Fe and Au in the catalyst was evident from STEM line analysis (Fig. S20). Solid state NMR revealed the atomic environment of the disordered structure of hydrophobic silica. For the HS, ^{29}Si (Fig. 5a) confirmed the presence of Q^2, Q^3, Q^4, and T^2, T^3 states[54,55]. When Fe was deposited using NaOH, Na atoms were incorporated in the silica matrix by making the Si-O-Na framework, confirmed by the decrement in the Q^3 and Q^2 states (Fig. 5b). A further decrease in Q^3 and Q^2 states was seen after the NaOH-assisted Au deposition (Fig. 5c). The Na 1s XPS spectrum confirmed the interaction of Si-O-Na (Fig. 5d) environment[56,57]. In the ^{23}Na NMR spectrum, 7.32 ppm and -1.59 ppm peaks confirmed the presence of Si-O-Na framework[58] (Fig. S21-S22). XPS and EDAX analysis supported the data. The pyridine-adsorbed FT-IR spectrum of the AuFeHS catalyst exhibits characteristic bands in the region 1400-1500 cm^{-1} (Fig. S23). The band at 1449 cm^{-1} are assigned to Lewis acid sites bonded to pyridine[59,60]. The band at ~1640 cm^{-1} is observed due to the –OH deformation vibrations and the physisorbed water molecules onto the surface of the materials[61]. It should be noted that the amount of physisorbed water over the hydrophobic catalyst was much less compared to SBA-15 (Fig. S3). The acidic sites on the bimetallic catalysts are crucial here and are well known for the C-H sigma complex for methane activation[62] and help in the regeneration of $Fe^{\delta+}$ sites[63]. The activated C-H sigma complex gets converted to CH_3 radical on the low valent $Fe^{3-\delta+}$ sites. Once the CH_3 and OH radicals are formed, methanol formation, facile CO insertion, and acetic acid generation become easy. It is imperative to conclude that Au nanoparticles, being excellent CO oxidation catalysts, provide low-energy activation sites for the adsorption of CO [64]. Even though we have optimized the catalysts based on bimetallic compositions, the role of Na and Lewis acid sites in the overall POM reaction is worth exploring and is beyond the scope of this study.

Conclusions: In summary, we have reported AuFeHS, a bimetallic catalyst supported on modified sodium containing silica (HS) for the continuous flow oxidation of methane to value-added products at ambient pressure and mild temperatures using H_2O_2 as an oxidant. The highly selective conversion of methane to methanol (>95%) with an yield of 1666 mmol/$g_{(Au+Fe)}$ within 30 min in batch process signs the presence of highly active sites in the material and the production of methanol in continuous flow process with a yield of 224 mmol/$g_{(Fe+Au)}$ opens the doors for the activation of methane at atmospheric conditions. While the synergistic effect between Au and Fe metals with sufficient acidic sites over silica support catalyzes the production of a high amount of methanol and acetic acid under benign conditions, care should be taken to prepare the support which helps to keep the peroxide radical close to the active metal sites. We believe that tuning active Fe species through a bimetallic modulation is a clever way to achieve catalytic conversion of lower alkanes to oxygenates, opening the scope for the commercialization of M2O (Methane to Oxygenates) technologies.

ASSOCIATED CONTENT

Supporting Information. Synthesis of HS, FeHS and AuFeHS, materials characterization methods, procedure and optimizations of the catalytic reactions, product calculation and XAS calculations, Activity data figures and tables.

Supporting Information should be included, ending with "This material is available free of charge via the Internet at http://pubs.acs.org."

AUTHOR INFORMATION

Corresponding Author

Dr. Vinod C Prabhakaran

[a] Catalysis and Inorganic Chemistry Division, CSIR-National Chemical Laboratory, Dr. Homi Bhabha Road, Pashan, Pune- 411008, India.

* Phone No.:+91-20-2590-2086, Email: cp.vinod@ncl.res.in

Author Contributions

CPV conceptualized the project, AVJ, PK and SG carried out the investigation, CPV obtained funding acquisition. CPV, TGA (NMR), SNJ and DB (EXAFS) did supervision. CPV, PK, AVJ and SG wrote the original draft and final writing – review & editing done by CPV, TGA (NMR), SNJ (EXAFS) and DB (EXAFS).

AVJ[$] and PK[$] contributed equally to this work

ACKNOWLEDGMENT

AVJ and PK thank CSIR and CSIR-UGC for the research fellowship. CPV thanks Director CSIR-NCL and the Council of Scientific and Industrial Research (CSIR) for funding through in-house grant MLP030626.

REFERENCES

(1) Luo, L.; Luo, J.; Li, H.; Ren, F.; Zhang, Y.; Liu, A.; Li, W.-X.; Zeng, J. Water Enables Mild Oxidation of Methane to Methanol on Gold Single-Atom Catalysts. *Nat Commun* **2021**, *12* (1), 1218. https://doi.org/10.1038/s41467-021-21482-z.

(2) Hamzehlouia, S.; Jaffer, S. A.; Chaouki, J. Microwave Heating-Assisted Catalytic Dry Reforming of Methane to Syngas. *Sci Rep* **2018**, *8* (1), 8940. https://doi.org/10.1038/s41598-018-27381-6.

(3) Latimer, A. A.; Kulkarni, A. R.; Aljama, H.; Montoya, J. H.; Yoo, J. S.; Tsai, C.; Abild-Pedersen, F.; Studt, F.; Nørskov, J. K. Understanding Trends in C–H Bond Activation in Heterogeneous Catalysis. *Nat Mater* **2017**, *16* (2), 225–229. https://doi.org/10.1038/nmat4760.

(4) Wu, B.; Lin, T.; Lu, Z.; Yu, X.; Huang, M.; Yang, R.; Wang, C.; Tian, C.; Li, J.; Sun, Y.; Zhong, L. Fe Binuclear Sites Convert Methane to Acetic Acid with Ultrahigh Selectivity. *Chem* **2022**, *8* (6), 1658–1672. https://doi.org/10.1016/j.chempr.2022.02.001.

(5) Qi, G.; Davies, T. E.; Nasrallah, A.; Sainna, M. A.; Howe, A. G. R.; Lewis, R. J.; Quesne, M.; Catlow, C. R. A.; Willock, D. J.; He, Q.; Bethell, D.; Howard, M. J.; Murrer, B. A.; Harrison, B.; Kiely, C. J.; Zhao, X.; Deng, F.; Xu, J.; Hutchings, G. J. Au-ZSM-5 Catalyses the Selective Oxidation of CH4 to CH3OH and CH3COOH Using O2. *Nat Catal* **2022**, *5* (1), 45–54. https://doi.org/10.1038/s41929-021-00725-8.

(6) Agarwal, N.; Freakley, S. J.; McVicker, R. U.; Althahban, S. M.; Dimitratos, N.; He, Q.; Morgan, D. J.; Jenkins, R. L.; Willock, D. J.; Taylor, S. H.; Kiely, C. J.; Hutchings, G. J. Aqueous Au-Pd Colloids Catalyze Selective CH_4 Oxidation to CH_3OH with O_2 under Mild Conditions. *Science (1979)* **2017**, *358* (6360), 223–227. https://doi.org/10.1126/science.aan6515.

(7) Xie, J.; Jin, R.; Li, A.; Bi, Y.; Ruan, Q.; Deng, Y.; Zhang, Y.; Yao, S.; Sankar, G.; Ma, D.; Tang, J. Highly Selective Oxidation of Methane to Methanol at Ambient Conditions by Titanium Dioxide-Supported Iron Species. *Nat Catal* **2018**, *1* (11), 889–896. https://doi.org/10.1038/s41929-018-0170-x.

(8) Narsimhan, K.; Iyoki, K.; Dinh, K.; Román-Leshkov, Y. Catalytic Oxidation of Methane into Methanol over Copper-Exchanged Zeolites with Oxygen at Low Temperature. *ACS Cent Sci* **2016**, *2* (6), 424–429. https://doi.org/10.1021/acscentsci.6b00139.

(9) Jin, Z.; Wang, L.; Zuidema, E.; Mondal, K.; Zhang, M.; Zhang, J.; Wang, C.; Meng, X.; Yang, H.; Mesters, C.; Xiao, F.-S. Hydrophobic Zeolite Modification for in Situ Peroxide Formation in Methane Oxidation to Methanol. *Science (1979)* **2020**, *367* (6474), 193–197. https://doi.org/10.1126/science.aaw1108.

(10) Xie, P.; Ding, J.; Yao, Z.; Pu, T.; Zhang, P.; Huang, Z.; Wang, C.; Zhang, J.; Zecher-Freeman, N.; Zong, H.; Yuan, D.; Deng, S.; Shahbazian-Yassar, R.; Wang, C. Oxo Dicopper Anchored on Carbon Nitride for Selective Oxidation of Methane. *Nat Commun* **2022**, *13* (1). https://doi.org/10.1038/s41467-022-28987-1.

(11) Ni, F.; Richards, T.; Smith, L. R.; Morgan, D. J.; Davies, T. E.; Lewis, R. J.; Hutchings, G. J. Selective Oxidation of Methane to Methanol via In Situ H_2O_2 Synthesis. *ACS Organic & Inorganic Au* **2023**. https://doi.org/10.1021/acsorginorgau.3c00001.

(12) Zhao, W.; Shi, Y.; Jiang, Y.; Zhang, X.; Long, C.; An, P.; Zhu, Y.; Shao, S.; Yan, Z.; Li, G.; Tang, Z. Fe-O Clusters Anchored on Nodes of Metal–Organic Frameworks for Direct Methane Oxidation. *Angewandte Chemie - International Edition* **2021**, *60* (11), 5811–5815. https://doi.org/10.1002/anie.202013807.

(13) Zhou, H.; Liu, T.; Zhao, X.; Zhao, Y.; Lv, H.; Fang, S.; Wang, X.; Zhou, F.; Xu, Q.; Xu, J.; Xiong, C.; Xue, Z.; Wang, K.; Cheong, W.; Xi, W.; Gu, L.; Yao, T.; Wei, S.; Hong, X.; Luo, J.; Li, Y.; Wu, Y. A Supported Nickel Catalyst Stabilized by a Surface Digging Effect for Efficient Methane Oxidation. *Angewandte Chemie* **2019**, *131* (51), 18559–18564. https://doi.org/10.1002/ange.201912785.

(14) Ab Rahim, M. H.; Armstrong, R. D.; Hammond, C.; Dimitratos, N.; Freakley, S. J.; Forde, M. M.; Morgan, D. J.; Lalev, G.; Jenkins, R. L.; Lopez-Sanchez, J. A.; Taylor, S. H.; Hutchings, G. J. Low Temperature Selective Oxidation of Methane to Methanol Using Titania Supported Gold Palladium Copper Catalysts. *Catal Sci Technol* **2016**, *6* (10), 3410–3418. https://doi.org/10.1039/c5cy01586c.

(15) Yuan, J.; Zhang, W.; Li, X.; Yang, J. A High Performance Catalyst for Methane Conversion to Methanol: Graphene Supported Single Atom Co. *Chemical Communications* **2018**, *54* (18), 2284–2287. https://doi.org/10.1039/c7cc08713f.

(16) Wang, A.; Li, J.; Zhang, T. Heterogeneous Single-Atom Catalysis. *Nature Reviews Chemistry*. Nature Publishing Group June 1, 2018, pp 65–81. https://doi.org/10.1038/s41570-018-0010-1.

(17) Shen, Q.; Cao, C.; Huang, R.; Zhu, L.; Zhou, X.; Zhang, Q.; Gu, L.; Song, W. Single Chromium Atoms Supported on Titanium Dioxide Nanoparticles for Synergic Catalytic Methane Conversion under Mild Conditions. *Angewandte Chemie* **2020**, *132* (3), 1232–1235. https://doi.org/10.1002/ange.201913309.

(18) Cui, X.; Li, H.; Wang, Y.; Hu, Y.; Hua, L.; Li, H.; Han, X.; Liu, Q.; Yang, F.; He, L.; Chen, X.; Li, Q.; Xiao, J.; Deng, D.; Bao, X. Room-Temperature Methane Conver-

sion by Graphene-Confined Single Iron Atoms. *Chem* **2018**, *4* (8), 1902–1910. https://doi.org/10.1016/j.chempr.2018.05.006.

(19) Osadchii, D. Y.; Olivos-Suarez, A. I.; Szécsényi, Á.; Li, G.; Nasalevich, M. A.; Dugulan, I. A.; Crespo, P. S.; Hensen, E. J. M.; Veber, S. L.; Fedin, M. V.; Sankar, G.; Pidko, E. A.; Gascon, J. Isolated Fe Sites in Metal Organic Frameworks Catalyze the Direct Conversion of Methane to Methanol. *ACS Catal* **2018**, *8* (6), 5542–5548. https://doi.org/10.1021/acscatal.8b00505.

(20) Bai, S.; Liu, F.; Huang, B.; Li, F.; Lin, H.; Wu, T.; Sun, M.; Wu, J.; Shao, Q.; Xu, Y.; Huang, X. High-Efficiency Direct Methane Conversion to Oxygenates on a Cerium Dioxide Nanowires Supported Rhodium Single-Atom Catalyst. *Nat Commun* **2020**, *11* (1). https://doi.org/10.1038/s41467-020-14742-x.

(21) Antil, N.; Chauhan, M.; Akhtar, N.; Newar, R.; Begum, W.; Malik, J.; Manna, K. Metal−Organic Framework-Encaged Monomeric Cobalt(III) Hydroperoxides Enable Chemoselective Methane Oxidation to Methanol. *ACS Catal* **2022**, *12* (18), 11159–11168. https://doi.org/10.1021/acscatal.2c02823.

(22) Tang, X.; Wang, L.; Yang, B.; Fei, C.; Yao, T.; Liu, W.; Lou, Y.; Dai, Q.; Cai, Y.; Cao, X. M.; Zhan, W.; Guo, Y.; Gong, X. Q.; Guo, Y. Direct Oxidation of Methane to Oxygenates on Supported Single Cu Atom Catalyst. *Appl Catal B* **2021**, *285*. https://doi.org/10.1016/j.apcatb.2020.119827.

(23) Grundner, S.; Markovits, M. A. C.; Li, G.; Tromp, M.; Pidko, E. A.; Hensen, E. J. M.; Jentys, A.; Sanchez-Sanchez, M.; Lercher, J. A. Single-Site Trinuclear Copper Oxygen Clusters in Mordenite for Selective Conversion of Methane to Methanol. *Nat Commun* **2015**, *6*. https://doi.org/10.1038/ncomms8546.

(24) Huang, W.; Zhang, S.; Tang, Y.; Li, Y.; Nguyen, L.; Li, Y.; Shan, J.; Xiao, D.; Gagne, R.; Frenkel, A. I.; Tao, F. F. Low-Temperature Transformation of Methane to Methanol on Pd 1 O 4 Single Sites Anchored on the Internal Surface of Microporous Silicate . *Angewandte Chemie* **2016**, *128* (43), 13639–13643. https://doi.org/10.1002/ange.201604708.

(25) Shan, J.; Li, M.; Allard, L. F.; Lee, S.; Flytzani-Stephanopoulos, M. Mild Oxidation of Methane to Methanol or Acetic Acid on Supported Isolated Rhodium Catalysts. *Nature* **2017**, *551* (7682), 605–608. https://doi.org/10.1038/nature24640.

(26) Narsimhan, K.; Iyoki, K.; Dinh, K.; Román-Leshkov, Y. Catalytic Oxidation of Methane into Methanol over Copper-Exchanged Zeolites with Oxygen at Low Temperature. *ACS Cent Sci* **2016**, *2* (6), 424–429. https://doi.org/10.1021/acscentsci.6b00139.

(27) Xu, J.; Armstrong, R. D.; Shaw, G.; Dummer, N. F.; Freakley, S. J.; Taylor, S. H.; Hutchings, G. J. Continuous Selective Oxidation of Methane to Methanol over Cu- and Fe-Modified ZSM-5 Catalysts in a Flow Reactor. *Catal Today* **2016**, *270*, 93–100. https://doi.org/10.1016/j.cattod.2015.09.011.

(28) Álvarez, M.; Marín, P.; Ordóñez, S. Harnessing of Diluted Methane Emissions by Direct Partial Oxidation of Methane to Methanol over Cu/Mordenite. *Ind Eng Chem Res* **2021**, *60* (26), 9409–9417. https://doi.org/10.1021/acs.iecr.1c01069.

(29) Xu, R.; Liu, N.; Dai, C.; Li, Y.; Zhang, J.; Wu, B.; Yu, G.; Chen, B. H $_2$ O-Built Proton Transfer Bridge Enhances Continuous Methane Oxidation to Methanol over Cu-BEA Zeolite. *Angewandte Chemie International Edition* **2021**, *60* (30), 16634–

16640. https://doi.org/10.1002/anie.202105167.

(30) Yang, G. S.; Kang, J.; Park, E. D. Aqueous-Phase Partial Oxidation of Methane over Pd−Fe/ZSM-5 with O_2 in the Presence of H_2. *ChemCatChem* **2023**, *15* (7). https://doi.org/10.1002/cctc.202201630.

(31) Soni, Y.; Pradhan, S.; Bamnia, M. K.; Yadav, A. K.; Jha, S. N.; Bhattacharyya, D.; Khan, T. S.; Haider, M. A.; Vinod, C. P. Spectroscopic Evidences for the Size Dependent Generation of Pd Species Responsible for the Low Temperature CO Oxidation Activity on Pd-SBA-15 Nanocatalyst. *Appl Catal B* **2020**, *272*, 118934. https://doi.org/10.1016/j.apcatb.2020.118934.

(32) Freakley, S. J.; Kochius, S.; van Marwijk, J.; Fenner, C.; Lewis, R. J.; Baldenius, K.; Marais, S. S.; Opperman, D. J.; Harrison, S. T. L.; Alcalde, M.; Smit, M. S.; Hutchings, G. J. A Chemo-Enzymatic Oxidation Cascade to Activate C–H Bonds with in Situ Generated H2O2. *Nat Commun* **2019**, *10* (1), 4178. https://doi.org/10.1038/s41467-019-12120-w.

(33) Lyu, J.; Niu, L.; Shen, F.; Wei, J.; Xiang, Y.; Yu, Z.; Zhang, G.; Ding, C.; Huang, Y.; Li, X. In Situ Hydrogen Peroxide Production for Selective Oxidation of Benzyl Alcohol over a Pd@Hierarchical Titanium Silicalite Catalyst. *ACS Omega* **2020**, *5* (27), 16865–16874. https://doi.org/10.1021/acsomega.0c02065.

(34) Wang, H.; Xin, W.; Wang, Q.; Zheng, X.; Lu, Z.; Pei, R.; He, P.; Dong, X. Direct Methane Conversion with Oxygen and CO over Hydrophobic DB-ZSM-5 Supported Rh Single-Atom Catalyst. *Catal Commun* **2022**, *162*, 106374. https://doi.org/10.1016/j.catcom.2021.106374.

(35) Daté, M.; Haruta, M. Moisture Effect on CO Oxidation over Au/TiO2 Catalyst. *J Catal* **2001**, *201* (2), 221–224. https://doi.org/10.1006/jcat.2001.3254.

(36) Daté, M.; Okumura, M.; Tsubota, S.; Haruta, M. Vital Role of Moisture in the Catalytic Activity of Supported Gold Nanoparticles. *Angewandte Chemie - International Edition* **2004**, *43* (16), 2129–2132. https://doi.org/10.1002/anie.200453796.

(37) Sun, G.; Jin, Y.; Zhang, Z.; Wang, Z.; Chai, P.; Xiong, F.; Huang, W. The Double-Edged Sword Effect of Water in the Low-Temperature CO Oxidation on Pt(111) Surface. *Journal of Physical Chemistry C* **2018**, *122* (39), 22530–22537. https://doi.org/10.1021/acs.jpcc.8b06500.

(38) Ikbal, S. A.; Colomban, C.; Zhang, D.; Delecluse, M.; Brotin, T.; Dufaud, V.; Dutasta, J.-P.; Sorokin, A. B.; Martinez, A. Bio-inspired Oxidation of Methane in the Confined Spaces of Molecular Cages. *Inorg Chem* **2019**, *58* (11), 7220–7228. https://doi.org/10.1021/acs.inorgchem.9b00199.

(39) Claveau, E. E.; Sader, S.; Jackson, B. A.; Khan, S. N.; Miliordos, E. Transition Metal Oxide Complexes as Molecular Catalysts for Selective Methane to Methanol Transformation: Any Prospects or Time to Retire? *Physical Chemistry Chemical Physics* **2023**, *25* (7), 5313–5326. https://doi.org/10.1039/D2CP05480A.

(40) Liu, J.-C.; Wang, Y.-G.; Li, J. Toward Rational Design of Oxide-Supported Single-Atom Catalysts: Atomic Dispersion of Gold on Ceria. *J Am Chem Soc* **2017**, *139* (17), 6190–6199. https://doi.org/10.1021/jacs.7b01602.

(41) Zhang, H.; Liu, G.; Shi, L.; Ye, J. Single-Atom Catalysts: Emerging Multifunctional Materials in Heterogeneous Catalysis. *Adv Energy Mater* **2018**, *8* (1), 1701343. https://doi.org/10.1002/aenm.201701343.

(42) Yang, T.; Meng, L.; Han, S.; Hou, J.; Wang, S.; Wang, X. Simultaneous Reductive and Sorptive Removal of Cr(

<scp>vi</Scp>) by Activated Carbon Supported β-FeOOH. *RSC Adv* **2017**, *7* (55), 34687–34693. https://doi.org/10.1039/C7RA06440C.

(43) Simons, M. C.; Prinslow, S. D.; Babucci, M.; Hoffman, A. S.; Hong, J.; Vitillo, J. G.; Bare, S. R.; Gates, B. C.; Lu, C. C.; Gagliardi, L.; Bhan, A. Beyond Radical Rebound: Methane Oxidation to Methanol Catalyzed by Iron Species in Metal–Organic Framework Nodes. *J Am Chem Soc* **2021**, *143* (31), 12165–12174. https://doi.org/10.1021/jacs.1c04766.

(44) Vitillo, J. G.; Bhan, A.; Cramer, C. J.; Lu, C. C.; Gagliardi, L. Quantum Chemical Characterization of Structural Single Fe(II) Sites in MIL-Type Metal–Organic Frameworks for the Oxidation of Methane to Methanol and Ethane to Ethanol. *ACS Catal* **2019**, *9* (4), 2870–2879. https://doi.org/10.1021/acscatal.8b04813.

(45) Sun, S.; Barnes, A. J.; Gong, X.; Lewis, R. J.; Dummer, N. F.; Bere, T.; Shaw, G.; Richards, N.; Morgan, D. J.; Hutchings, G. J. Lanthanum Modified Fe-ZSM-5 Zeolites for Selective Methane Oxidation with H_2O_2. *Catal Sci Technol* **2021**, *11* (24), 8052–8064. https://doi.org/10.1039/D1CY01643A.

(46) Szécsényi, Á.; Li, G.; Gascon, J.; Pidko, E. A. Mechanistic Complexity of Methane Oxidation with H_2O_2 by Single-Site Fe/ZSM-5 Catalyst. *ACS Catal* **2018**, *8* (9), 7961–7972. https://doi.org/10.1021/acscatal.8b01672.

(47) Meunier, F. C. Relevance of IR Spectroscopy of Adsorbed CO for the Characterization of Heterogeneous Catalysts Containing Isolated Atoms. *The Journal of Physical Chemistry C* **2021**, *125* (40), 21810–21823. https://doi.org/10.1021/acs.jpcc.1c06784.

(48) Calle-Vallejo, F.; Tymoczko, J.; Colic, V.; Vu, Q. H.; Pohl, M. D.; Morgenstern, K.; Loffreda, D.; Sautet, P.; Schuhmann, W.; Bandarenka, A. S. Finding Optimal Surface Sites on Heterogeneous Catalysts by Counting Nearest Neighbors. *Science (1979)* **2015**, *350* (6257), 185–189. https://doi.org/10.1126/science.aab3501.

(49) Wang, X.; Rosspeintner, A.; Ziarati, A.; Zhao, J.; Bürgi, T. Insight into the Transient Inactivation Effect on Au/TiO2 Catalyst by in-Situ DRIFT and UV–Vis Spectroscopy. *Nat Commun* **2022**, *13* (1), 5458. https://doi.org/10.1038/s41467-022-33187-y.

(50) Wei, S.; Fu, X.-P.; Wang, W.-W.; Jin, Z.; Song, Q.-S.; Jia, C.-J. Au/TiO_2 Catalysts for CO Oxidation: Effect of Gold State to Reactivity. *The Journal of Physical Chemistry C* **2018**, *122* (9), 4928–4936. https://doi.org/10.1021/acs.jpcc.7b12418.

(51) Yu, T.; Li, Z.; Lin, L.; Chu, S.; Su, Y.; Song, W.; Wang, A.; Weckhuysen, B. M.; Luo, W. Highly Selective Oxidation of Methane into Methanol over Cu-Promoted Monomeric Fe/ZSM-5. *ACS Catal* **2021**, *11* (11), 6684–6691. https://doi.org/10.1021/acscatal.1c00905.

(52) Hammond, C.; Forde, M. M.; Ab Rahim, M. H.; Thetford, A.; He, Q.; Jenkins, R. L.; Dimitratos, N.; Lopez-Sanchez, J. A.; Dummer, N. F.; Murphy, D. M.; Carley, A. F.; Taylor, S. H.; Willock, D. J.; Stangland, E. E.; Kang, J.; Hagen, H.; Kiely, C. J.; Hutchings, G. J. Direct Catalytic Conversion of Methane to Methanol in an Aqueous Medium by Using Copper-Promoted Fe-ZSM-5. *Angewandte Chemie International Edition* **2012**, *51* (21), 5129–5133. https://doi.org/10.1002/anie.201108706.

(53) Tang, Y.; Li, Y.; (Feng) Tao, F. Activation and Catalytic Transformation of Methane under Mild Conditions. *Chem Soc Rev* **2022**, *51* (1), 376–423. https://doi.org/10.1039/D1CS00783A.

(54) Protsak, I. S.; Morozov, Y. M.; Dong, W.; Le, Z.; Zhang, D.; Henderson, I. M. A 29Si, 1H, and 13C Solid-State NMR Study on the Surface Species of Various Depol-

ymerized Organosiloxanes at Silica Surface. *Nanoscale Res Lett* **2019**, *14* (1), 160. https://doi.org/10.1186/s11671-019-2982-2.

(55) Gadzała-Kopciuch, R.; Kluska, M.; Wełniak, M.; Buszewski, B. Silicon Dioxide Surfaces with Aryl Interaction Sites for Chromatographic Applications. *Mater Chem Phys* **2005**, *89* (2–3), 228–237. https://doi.org/10.1016/j.matchemphys.2004.03.022.

(56) Mekki, A.; Holland, D.; McConville, C. F.; Salim, M. An XPS Study of Iron Sodium Silicate Glass Surfaces. *J Non Cryst Solids* **1996**, *208* (3), 267–276. https://doi.org/10.1016/S0022-3093(96)00523-6.

(57) Dong, B.; Xu, Y.; Lin, S.; Dai, X. Characterizing and Exploring the Formation Mechanism of Salt Deposition by Reusing Advanced-Softened, Silica-Rich, Oilfield-Produced Water (ASOW) in Superheated Steam Pipeline. *Sci Rep* **2015**, *5* (1), 17274. https://doi.org/10.1038/srep17274.

(58) Koller, H.; Engelhardt, G.; Kentgens, A. P. M.; Sauer, J. 23Na NMR Spectroscopy of Solids: Interpretation of Quadrupole Interaction Parameters and Chemical Shifts. *J Phys Chem* **1994**, *98* (6), 1544–1551. https://doi.org/10.1021/j100057a004.

(59) Li, Y.; Zhang, W.; Zhang, L.; Yang, Q.; Wei, Z.; Feng, Z.; Li, C. Direct Synthesis of Al−SBA-15 Mesoporous Materials via Hydrolysis-Controlled Approach. *J Phys Chem B* **2004**, *108* (28), 9739–9744. https://doi.org/10.1021/jp049824j.

(60) Udayakumar, V.; Pandurangan, A. Synthesis of Hf/SBA-15 Lewis Acid Catalyst for Converting Glycerol to Value-Added Chemicals. *Journal of Porous Materials* **2017**, *24* (4), 979–990. https://doi.org/10.1007/s10934-016-0337-2.

(61) Gabla, J. J.; Lathiya, D. R.; Revawala, A. A.; Maheria, K. C. Propyl–SO3H Functionalized SBA-15: Microwave-Mediated Green Synthesis of Biologically Active Multi-Substituted Imidazole Scaffolds. *Research on Chemical Intermediates* **2019**, *45* (4), 1863–1881. https://doi.org/10.1007/s11164-018-3707-3.

(62) Raynes, S.; Shah, M. A.; Taylor, R. A. Direct Conversion of Methane to Methanol with Zeolites: Towards Understanding the Role of Extra-Framework d-Block Metal and Zeolite Framework Type. *Dalton Transactions* **2019**, *48* (28), 10364–10384. https://doi.org/10.1039/C9DT00922A.

(63) Krisnandi, Y. K.; Nurani, D. A.; Alfian, D. V.; Sofyani, U.; Faisal, M.; Saragi, I. R.; Pamungkas, A. Z.; Pratama, A. P. The New Challenge of Partial Oxidation of Methane over Fe2O3/NaY and Fe3O4/NaY Heterogeneous Catalysts. *Heliyon* **2021**, *7* (11), e08305. https://doi.org/10.1016/j.heliyon.2021.e08305.

(64) Ha, H.; Yoon, S.; An, K.; Kim, H. Y. Catalytic CO Oxidation over Au Nanoparticles Supported on CeO_2 Nanocrystals: Effect of the Au–CeO_2 Interface. *ACS Catal* **2018**, *8* (12), 11491–11501. https://doi.org/10.1021/acscatal.8b03539.